Charles University in Prague
First Faculty of Medicine

Institute of Physiology
Academy of Sciences of the Czech Republic

Neuronal excitability, properties of native NMDA receptors, their modulation by physical and chemical factors

Miloslav Sedláček

Summary of PhD Thesis

Prague 2007

Applicant: Miloslav Sedláček
Address: Department of Cellular Neurophysiology
Institute of Physiology AS CR, v.v.i.
Vídeňská 1083
142 20 Prague 4
phone: 00420 2 4106 2543
fax: 00420 2 4106 2488

Commission: Neuroscience

Supervisor: Ladislav Vyklický Jr., M.D., D.Sc.

Opponents:

Summary was sent out on:

Defence of the Thesis:

Chairman of the Commission:

7. List of publications:

Published in impacted journals:

1. Krusek J, Dittert I, Hendrych T, Hnik P, Horak M, Petrovic M, Sedlacek M, Susankova K, Svobodova L, Tousova K, Ujec E, Vlachova V, Vyklicky L, Vyskocil F, Vyklicky L Jr. (2004) Activation and modulation of ligand-gated ion channels. Physiol Res. 53, S103-13. (IF 2.093)

2. Petrovic M, Sedlacek M, Horak M., Chodounska H, Vyklicky L Jr. (2005) 20-oxo-5β-pregnan-3α-yl sulfate is a use-dependent NMDA receptor inhibitor. J Neurosci; Sep 14; 25 (37): 8439-50 (IF 7.453)

3. Sedlacek M, Horak M, Vyklicky L Jr. (2007) Morphology and physiology of lamina I neurons of the caudal part of the trigeminal nucleus. Neuroscience; Jun 29; 147 (2): 325-333 (IF 3.427)

4. Cais O, Sedlacek M, Horak M, Dittert I, Vyklicky L Jr. (2007) Temperature dependence of NR1/NR2B NMDA receptor. Accepted. Neuroscience. (IF 3.427)

Other publications:

1. Sedláček, M., Horák, M., Petrovič, M., Vyklický, L. Jr. (2003) NMDA receptory a důsledky jejich farmakologického ovlivnění. Psychiatrie 7 (Supplementum 3; Původní práce), 41-45.

2. Petrovič, M., Sedláček, M., Horák, M., Vyklický, L. Jr. (2004) Neurofarmakologická podstata působení memantinu v léčbě Alzheimerovy demence. Klinická farmakologie a farmacie 18, 81-89.

3. Vyklický, L. Jr., Horák, M., Petrovič, M., Sedláček, M., Sušánková, K., Toušová, K., Vyklický, L. Sn. a Vlachová, V. (2004) Iontové kanály a modulace jejich aktivity fyzikálními a chemickými podněty. Psychiatrie 8 (Suplementum 3, původní práce); 6-12.

4. Petrovic M, Horak M, Sedlacek M, Vyklicky L Jr. (2005) Physiology and Pathology of NMDA Receptors. Prague Medical Report Vol. 106, No. 2., 113-136. Review

1. Introduction

NMDA receptors (NMDARs) are glutamate-gated Ca^{2+}-permeable ion channels. Their slow activation and deactivation kinetics make NMDARs important contributors to long-term synaptic plasticity and excitotoxicity. These receptors are probably heterotetramers composed of two NR1 subunits in combination with NR2A – D and/or NR3A, B subunits. The subunits share the same topology: extracellularly located N-terminus, three fully transmembrane domains, one forming a re-entrant loop, and an intracellular C terminus. NMDA receptors possess two distinct binding sites for agonists - glycine and glutamate (for a review see Dingledine et al., 1999).

NMDARs are expressed in the nervous system of a broad range of animals, including early metazoans (Pierobon et al., 2004) and higher vertebrates, both ectothermic and endothermic (see e.g Davies et al., 1979; Dale and Roberts, 1984). While in invertebrates and lower vertebrates neurons operate at wide temperature range, from slightly above 0 to over 40°C, mammalian neurons are adapted to operate at a narrow range of temperatures, usually between 35 and 40°C (Ederstrom, 1973; Samis et al., 1973; Simmonds, 1973). The functional and pharmacological properties of NMDARs, including those synaptically activated, have been determined mainly at room temperature. Although such temperature is physiological for many lower vertebrate species, these conditions are at least 10°C below physiological for mammalian neurons.

NMDA receptor activity can be influenced by exogenous and endogenous ligands, including neurosteroids. These compounds are of steroid origin, having a direct nongenomic effect on neuronal excitability (Paul and Purdy, 1992). They are both synthesized *de novo* in the central nervous system (CNS), and modified to neuroactive compounds from circulating precursors and can reach high local concentrations (Mellon and Griffin, 2002; Kawato et al., 2003). It has been well established that neurosteroids exert a positive, negative or combined effect on NMDA receptors (Wu et al., 1991; Bowlby, 1993; Park-Chung et al., 1994; Horak et al., 2004). Pregnenolone sulfate (PS), an endogenously occurring neurosteroid, acts in a subunit-dependent manner as a combined positive and negative modulator of NMDA receptors (Malayev et al., 2002; Horak et al., 2004). The mechanism of action of PS associated with a positive effect is

disuse-dependent (i.e. NMDA receptor affinity for PS is decreased upon receptor activation) and involves an increase in the peak probability of the NMDA receptor opening (P_o). In contrast, 20-oxo-5β-pregnan-3α-yl sulphate (pregnanolone sulfate, 3α5βS), also a naturally occurring neurosteroid that differs from PS in a single unsaturated bond, has an inhibitory action at NMDA receptors (Park-Chung et al., 1994). Even though the molecular mechanism of 3α5βS action at NMDA receptors is only partially understood, its synthetic analog 3α5β hemisuccinate ester has been shown to have a neuroprotective effect, both *in vitro* (hippocampal neurons) and *in vivo* (spinal cord ischemia model), thereby indicating its potential therapeutic use (Weaver et al., 1998; Lapchak, 2004).

The intrinsic membrane properties of neurons, which are fundamental in determining how a neuron will respond to a specific input (for a review, see Hille, 1992), vary widely between cell types of the mammalian nervous system (Llinas, 1988). In general, many types of neurons exist in the mammalian CNS, differing by their membrane properties, various neurotransmitter systems and ion channels expression. All of these characteristics determine, how a neuron will respond to an afferent input (Crill and Schwindt, 1984; Gustafsson, 1984; Morisset and Nagy, 1998; Engel et al., 1999), how this information will be analyzed, and finally, what efferent output will arise. Various firing patterns have been described for different neuronal populations in the CNS with tonic or phasic activity, or a combination of both (Schwindt and Crill, 1999; Williams and Stuart, 1999; Sherman, 2001; Grudt and Perl, 2002; Prescott and De Koninck, 2002; Ruscheweyh and Sandkuhler, 2002). The bursting as a response to sensory stimuli is based on specific cellular mechanisms, which are supposed to be regulated by feedback synaptic inputs coming from the same neuron or other neurons of a local circuit. For the mammalian sensory system, tonic and phasic firing patterns are likely to form a complex code for signal transduction (for a review see Krahe and Gabbiani, 2004).

It has been shown, that the dendritic arborization of neurons determines, how a neuron generates action potentials (Mainen and Sejnowski, 1996). The transition between the tonic activity and various degrees of bursting is strongly dependent upon the

Samis HV, Baird MB, Lints FA (1973) 99. Life span and temperature: Insects. In: Biology data book, Second Edition Edition (Dittmer DS, ed), p p. 873. Bethesda: Federation of American Societies for Experimental Biology.

Schwindt P, Crill W (1999) Mechanisms underlying burst and regular spiking evoked by dendritic depolarization in layer 5 cortical pyramidal neurons. J Neurophysiol 81:1341-1354.

Sherman SM (2001) Tonic and burst firing: dual modes of thalamocortical relay. Trends in Neurosciences 24:122-126.

Simmonds RC (1973) 98. Metabolism and temperature: Hibernating mammals and birds. In: Biology data book, Second Edition Edition (Dittmer DS, ed), pp 870-873. Bethesda: Federation of American Societies for Experimental Biology.

Tamaoki T, Nomoto H, Takahashi I, Kato Y, Morimoto M, Tomita F (1986) Staurosporine, a potent inhibitor of phospholipid/Ca++dependent protein kinase. Biochem Biophys Res Commun 135:397-402.

Vyklicky L, Jr., Benveniste M, Mayer ML (1990) Modulation of N-methyl-D-aspartic acid receptor desensitization by glycine in mouse cultured hippocampal neurones. J Physiol Lond 428:313-331.

Weaver CE, Jr., Wu FS, Gibbs TT, Farb DH (1998) Pregnenolone sulfate exacerbates NMDA-induced death of hippocampal neurons. Brain Res 803:129-136.

Williams K (1993) Ifenprodil discriminates subtypes of the N-methyl-D-aspartate receptor: selectivity and mechanisms at recombinant heteromeric receptors. Mol Pharmacol 44:851-859.

Williams SR, Stuart GJ (1999) Mechanisms and consequences of action potential burst firing in rat neocortical pyramidal neurons. J Physiol (Lond) 521:467-482.

Wu F, Gibbs T, Farb D (1991) Pregnenolone sulfate: a positive allosteric modulator at the N-methyl-D- aspartate receptor. Mol Pharmacol 40:333-336.

Yanagihara N, Tachikawa E, Izumi F, Yasugawa S, Yamamoto H, Miyamoto E (1991) Staurosporine: an effective inhibitor for Ca2+/calmodulin-dependent protein kinase II. J Neurochem 56:294-298.

Zhang ET, Han ZS, Craig AD (1996) Morphological classes of spinothalamic lamina I neurons in the cat. J Comp Neurol 367:537-549.

Lapchak PA (2004) The neuroactive steroid 3-alpha-ol-5-beta-pregnan-20-one hemisuccinate, a selective NMDA receptor antagonist improves behavioral performance following spinal cord ischemia. Brain Res 997:152-158.
Lima D, Coimbra A (1986) A Golgi study of the neuronal population of the marginal zone (lamina I) of the rat spinal cord. J Comp Neurol 244:53-71.
Llinas RR (1988) The intrinsic electrophysiological properties of mammalian neurons: insights into central nervous system function. Science 242:1654-1664.
Mainen ZF, Sejnowski TJ (1996) Influence of dendritic structure on firing pattern in model neocortical neurons. Nature 382:363-366.
Malayev A, Gibbs TT, Farb DH (2002) Inhibition of the NMDA response by pregnenolone sulphate reveals subtype selective modulation of NMDA receptors by sulphated steroids. Br J Pharmacol 135:901-909.
Mason A, Larkman A (1990) Correlations between morphology and electrophysiology of pyramidal neurons in slices of rat visual cortex. II. Electrophysiology. J Neurosci 10:1415-1428.
Mellon SH, Griffin LD (2002) Synthesis, regulation, and function of neurosteroids. Endocr Res 28:463.
Monyer H, Burnashev N, Laurie DJ, Sakmann B, Seeburg PH (1994) Developmental and regional expression in the rat brain and functional properties of four NMDA receptors. Neuron 12:529-540.
Morisset V, Nagy F (1998) Nociceptive integration in the rat spinal cord: role of non-linear membrane properties of deep dorsal horn neurons. Eur J Neurosci 10:3642-3652.
Park-Chung M, Wu F, Farb D (1994) 3 alpha-Hydroxy-5 beta-pregnan-20-one sulfate: a negative modulator of the NMDA-induced current in cultured neurons. Mol Pharmacol 46:146-150.
Park-Chung M, Wu FS, Purdy RH, Malayev AA, Gibbs TT, Farb DH (1997) Distinct sites for inverse modulation of N-methyl-D-aspartate receptors by sulfated steroids. Mol Pharmacol 52:1113-1123.
Paul SM, Purdy RH (1992) Neuroactive steroids. Faseb J 6:2311-2322.
Petrovic M, Sedlacek M, Horak M, Chodounska H, Vyklicky L, Jr. (2005) 20-oxo-5beta-pregnan-3alpha-yl sulfate is a use-dependent NMDA receptor inhibitor. J Neurosci 25:8439-8450.
Pierobon P, Sogliano C, Minei R, Tino A, Porcu P, Marino G, Tortiglione C, Concas A (2004) Putative NMDA receptors in Hydra: a biochemical and functional study. Eur J Neurosci 20:2598-2604.
Prescott SA, De Koninck Y (2002) Four cell types with distinctive membrane properties and morphologies in lamina I of the spinal dorsal horn of the adult rat. J Physiol 539:817-836.
Ruegg UT, Burgess GM (1989) Staurosporine, K-252 and UCN-01: potent but nonspecific inhibitors of protein kinases. Trends Pharmacol Sci 10:218-220.
Ruscheweyh R, Sandkuhler J (2002) Lamina-specific membrane and discharge properties of rat spinal dorsal horn neurones in vitro. J Physiol 541:231-244.

structure and extent of the dendritic tree (Connors and Gutnick, 1990; Mason and Larkman, 1990; Gray and McCormick, 1996).

Regarding the physiology and histology it has been shown, that the mammalian trigeminal sensory system has some features in common with the spinal cord sensory system (Gobel and Binck, 1977; Lima and Coimbra, 1986; Zhang et al., 1996). Several papers dealt with electrophysiological and morphological properties of superficial laminae of the spinal cord dorsal horn (Grudt and Perl, 2002; Prescott and De Koninck, 2002; Ruscheweyh and Sandkuhler, 2002). However, little evidence exists so far, as if neurons of lamina I of the trigeminal subnucleus caudalis (Sp5C) show the same or comparable membrane and morphological characteristics with the spinal cord dorsal horn lamina I neurons.

2. Experimental questions

The thesis was primarily focused at characterization of the functional and pharmacological properties of native NMDA receptors in acute brain slices and cultured hippocampal neurons. The general excitability, especially in the trigeminal sensory neurons was studied as well as their morphology. The specific aims of our experiments were to:

1. Characterize the temperature dependence of amplitude and deactivation kinetics of NMDA receptor mediated excitatory postsynaptic currents (NMDAR EPSCs) in pyramidal neurons in layer II/III of the rat neocortex.
2. Reveal the molecular mechanisms by which pregnanolone sulfate (3α5βS) modulates the synaptically activated NMDA receptors.
3. Characterize the effect of pregnenolon sulfate (PS) on synaptically activated NMDA receptors.
4. Characterize basic properties of the excitatory synaptic transmission between trigeminal tract and lamina I neurons in the trigeminal subnucleus caudalis (Sp5C).
5. Electrophysiologically characterize the active and passive membrane properties of Sp5C lamina I neurons and classify individual groups of neurons.

6. Analyze the morphological features of Sp5C lamina I neurons and classify neurons into groups.

3. Methods

All experiments were performed on acute brain slices prepared from the rat neocortex or trigeminal subnucleus caudalis (postnatal age of 2 weeks), and on cultured hippocampal neurons.

Trigeminal nucleus and neocortex slice preparation, solutions used

13- to 15-day-old Wistar rats of both sexes were used in the present study. The pups were decapitated under ether anaesthesia and the brainstem was dissected and immersed in ice-cold (<4°C) extracellular solution (ECS). Transverse slices, 300 μm in thickness, were cut from the medulla oblongata caudally to obex using a vibratome (DTK-1000, Dosaka EM Co., Kyoto, Japan). Slices containing the Sp5C were incubated in ECS at 34°C for one hour. Slices were maintained at room temperature (6-8 hours) before being placed in a recording chamber, where they were continually perfused with ECS at a rate of 3 ml/min.

For the purpose of the neocortical slices preparation, the animals, processes of anaesthesia, decapitation and cranial tissue preparation were the same as in the case of the trigeminal nucleus slices. For the neocortical slices preparation we routinely used the right hemisphere of the rat brain from which 300 μm tangential slices were cut using a vibratome (DTK-1000, Dosaka EM Co., Kyoto, Japan). The same procedure as in the case of the trigeminal nucleus was used for the neocortical slices incubation and storing after they were cut.

For both, the trigeminal nucleus and neocortical slices cutting, incubation and perfusion, ECS of the following composition (in mM) was used: 130 NaCl; 2.5 KCl; 28 $NaHCO_3$; 1.25 NaH_2PO_4; 1 $MgCl_2$; 2 $CaCl_2$; 25 glucose; pH 7.35; 320 mosmol; it was gassed with O_2 (95%)/CO_2 (5%).

6. References

Bowlby MR (1993) Pregnenolone sulfate potentiation of N-methyl-D-aspartate receptor channels in hippocampal neurons. Mol Pharmacol 43:813-819.

Connors BW, Gutnick MJ (1990) Intrinsic firing patterns of diverse neocortical neurons. Trends Neurosci 13:99-104.

Crill WE, Schwindt P (1984) Ionic mechanisms underlying excitation-to-frequency transduction: studies by voltage clamp methods. Arch Ital Biol 122:31-41.

Dale N, Roberts A (1984) Excitatory amino acid receptors in Xenopus embryo spinal cord and their role in the activation of swimming. J Physiol 348:527-543.

Davies J, Evans RH, Francis AA, Watkins JC (1979) Excitatory amino acid receptors and synaptic excitation in the mammalian central nervous system. J Physiol (Paris) 75:641-654.

Dingledine R, Borges K, Bowie D, Traynelis SF (1999) The glutamate receptor ion channels. Pharmacol Rev 51:7-61.

Ederstrom HE (1973) 95. Temperature characteristics: Homoiothermic animals. In: Biology data book, Second Edition Edition (Dittmer DS, ed), pp 863-864. Bethesda: Federation of American Societies for Experimental Biology.

Engel J, Schultens HA, Schild D (1999) Small conductance potassium channels cause an activity-dependent spike frequency adaptation and make the transfer function of neurons logarithmic. Biophys J 76:1310-1319.

Flint AC, Maisch US, Weishaupt JH, Kriegstein AR, Monyer H (1997) NR2A subunit expression shortens NMDA receptor synaptic currents in developing neocortex. J Neurosci 17:2469-2476.

Gobel S, Binck JM (1977) Degenerative changes in primary trigeminal axons and in neurons in nucleus caudalis following tooth pulp extirpations in the cat. Brain Res 132:347-354.

Gray CM, McCormick DA (1996) Chattering Cells: Superficial Pyramidal Neurons Contributing to the Generation of Synchronous Oscillations in the Visual Cortex. Science 274:109-113.

Grudt TJ, Perl ER (2002) Correlations between neuronal morphology and electrophysiological features in the rodent superficial dorsal horn. J Physiol 540:189-207.

Gustafsson B (1984) Afterpotentials and transduction properties in different types of central neurones. Arch Ital Biol 122:17-30.

Hille B (1992) Ionic Channels of Excitable Membranes. In. Sunderland, MA, USA: Sinauer Associates.

Horak M, Vlcek K, Petrovic M, Chodounska H, Vyklicky L, Jr. (2004) Molecular mechanism of pregnenolone sulfate action at NR1/NR2B receptors. J Neurosci 24:10318-10325.

Kawato S, Yamada M, Kimoto T (2003) Brain neurosteroids are 4th generation neuromessengers in the brain: cell biophysical analysis of steroid signal transduction. Adv Biophys 37:1-48.

Krahe R, Gabbiani F (2004) Burst firing in sensory systems. Nat Rev Neurosci 5:13-23.

dependent mechanism of 3α5βS action on NMDA receptors may have significant implications for the design of therapeutic agents with potential clinical use

3. Pregnenolon sulfate (PS) does not potentiate NMDAR EPSC amplitudes in layer II/III pyramidal neurons of the neocortex, in Sp5C lamina I neurons or in cultured hippocampal neurons. This is in contrast with robust potentiation of recombinant and native NMDA receptors of similar subunit composition published previously. We demonstrate that several intracellular mechanisms are likely to be included in the mechanisms of PS induced potentiation of responses of native NMDA receptors.

a) The results of our experiments indicate that the degree of phosphorylation/dephosphorylation of NMDA receptors determines the degree of PS induced potentiation since the incubation of cultured hippocampal neurons with staurosporine caused a significant reduction of PS induced potentiation.

b) The isolation of membrane patch from cultured hippocampal neurons strongly influences the degree of PS induced potentiation of NMDA responses.

4. a) The data we presented in this thesis show that Sp5C lamina I neurons comprise three morphological types - fusiform, pyramidal, and multipolar - and four functional types - tonic, phasic, delayed onset, and single spike.

b) Correlation between morphological and physiological types of neurons indicates that fusiform and pyramidal cells may correspond to tonic or phasic neurons, and multipolar cells to delayed onset or single spike neurons. In addition, the time course of excitatory synaptic input induced by primary afferent stimulation was quantitatively characterized. The results of our experiments suggest that physiological types of lamina I neurons with specific morphological and synaptic input characteristics present a basis for their functional integration in the processing and transduction of sensory information from the orofacial region.

Sp5C lamina I neurons histology and labeling

For the detailed morphological analysis of Sp5C lamina I neurons, a biocytin filling and Streptavidin-Alexa 488 labeling of the neurons protocol was used. After 45-60 min. of whole-cell recording, which was sufficient to allow biocytin diffusion from the patch-clamp pipette to the neuronal soma and dendrites, the pipette was withdrawn carefully from the cell and the slice was fixed (3% paraformaldehyde in 0.15 M sodium phosphate buffer; pH 7.3) at 4°C overnight. After thorough rinsing in PBS, the slices were incubated for 100 min. in Streptavidin Alexa Fluor® 488 (10 µg/ml; 5 µl/ml; Molecular Probes, Eugene, OR, USA) in PBS containing 0.4% Triton X-100. The slices were then rinsed 3×10 min. in PBS, dried overnight on a gelatin-coated slide, dehydrated (ethanol 75%, 90%, 95%, xylene; slices left in each solution for 2 min.), and coverslipped in a solution of mowiol with 2.5% 1,4-diazabicyclo[2.2.2] octane (DABCO). Single-photon confocal microscopy (MRC 600; Bio-Rad, Hercules, CA, USA) allowing excitation at 488 nm was used to acquire serial optical sections at 2 µm steps.

Hippocampal cultures

Primary dissociated hippocampal cultures were prepared from 1- to 2-day-old postnatal rat pups. Rats were decapitated, and the hippocampi were dissected. Trypsin digestion, followed by mechanical dissociation, was used to prepare a cell suspension. Single cells were plated at a density of 100,000 cells/cm^2 onto a confluent glial feeder layer prepared two weeks earlier. Neuronal cultures were maintained in a medium composed of MEM, 10% horse serum and a nutrient supplement consisting of transferrin, insulin, selenium, corticosterone, triiodothyronine, and progesterone. A metabolic inhibitor, 5-fluoro-2'-deoxyuridine, was used to suppress cell division.

Recordings, data acquisition and drugs application

Patch-clamp pipettes (3 - 5 MΩ) were made from borosilicate glass and filled with either K^+ based intracellular solution (K-ICS) for current clamp experiments or Cs^+ based intracellular solution (Cs-ICS) for voltage clamp experiments. K-ICS was composed

of (in mM): 107.5 K-gluconate; 32.5 KCl; 5 EGTA; 10 HEPES; 1 $MgCl_2$; 2 ATP-Mg salt; 0.5% biocytin; pH 7.2 adjusted with KOH. Cs-ICS was composed of (in mM): 125 gluconic acid, 15 CsCl; 5 EGTA; 10 HEPES; 3 $MgCl_2$; 0.5 $CaCl_2$; 2 ATP-Mg salt; pH-adjusted to 7.2 with CsOH. Whole-cell recordings were made from Sp5C lamina I neurons, neocortical layer II/III pyramidal neurons or cultured hippocampal neurons selected under visual control using an upright epifluorescence microscope (Axioskop-FS, Zeiss, Germany) equipped with infrared "gradient contrast" optics (Dodt et al., 1998) and a 63x0.75 NA water-immersion lens (for the case of the acute slices) or an inverted microscope (Nikon) (for the case of neuronal tissue cultures).

Whole-cell recordings in current-clamp or voltage-clamp mode were obtained with a patch-clamp amplifier Axopatch 200B (Axon Instruments, Inc., Foster City, CA, USA). Reported values of membrane potential (V_m) were corrected for the liquid junction potential, which was +6 mV for K-ICS and +9.5 mV for Cs-ICS. The voltage and current output were low-pass filtered at 1 or 2 kHz with an 8-pole Bessel filter (Frequency Devices, Haverhill, MA, USA), digitally sampled at 5 or 10 kHz. To elicit AMPA or NMDA receptor-mediated EPSCs, a glass pipette (similar to that used for patch-clamp recording) filled with an extracellular solution and placed in the spinal trigeminal tract or layer I in the case of neocortex near (20-100 μm) the postsynaptic neuron was used to deliver stimuli of 15-30 μA with a duration of 0.5 ms. The stimuli were applied at 5 s (AMPA receptor-mediated EPSCs) or 20 s (NMDA receptor-mediated EPSCs) intervals from an Isolator 11 (Axon Instruments). To elecit the postsynaptic currents among pairs of cultured hippocampal neurons we used a pipette filled with the extracellular solution and electrically connected to a stimulator (W-P Instruments, USA) to stimulate the presynaptic neuron, and a recording pipette filled with the cesium based ICS to record the postsynaptic currents.

ECS of the following composition were used for recordings from cultured neurons (in mM):

Perfusing ECS: NaCl, 160; KCl, 2.5; HEPES, 10; glucose, 10; $MgCl_2$, 1; $CaCl_2$, 2; ECS for applications: NaCl, 160; KCl, 2.5; HEPES, 10; glucose, 10; $CaCl_2$, 0.2; pH was adjusted to 7.3 with NaOH, osmolarity 315-325 mOsm.

5. Conclusions

The present thesis was focused at the study of functional and pharmacological properties of native and synaptically activated NMDA receptors, and at the study of electrophysiological and morphological characteristics of neurons of the trigeminal sensory system. The results of experiments can be summarized into the following points:

1. We demonstrate that the amplitude and deactivation time course of NMDAR EPSCs are temperature dependent.

a) We show that the amplitude increase (of both the miniature and evoked NMDAR EPSCs) with higher temperature is determined by the increased NMDAR channel conductance.

b) The kinetics of NMDAR EPSCs deactivation shortens with higher temperature. The temperature coefficient (Q_{10}) for both the fast and slow component of decay is, however, of somewhat lower value than that of recombinant NR1/NR2B NMDA receptors co-expressed in HEK 293 cells. NR2B selective antagonist ifenprodil does not significantly change the basic characteristics of deactivation kinetics of evoked NMDAR EPSCs neither at room, nor at physiological temperatures. This suggests that the decay of NMDAR EPSCs cannot be simply explained by the presence of receptors with subunit combinations of NR1/NR2A or NR1/NR2B in synapses.

2. We demonstrate that 3α5βS is a voltage-independent inhibitor of synaptically activated NMDA receptors in layer II/III pyramidal neurons of the neocortex. Based on the results of our experiments we conclude that this compound is a use-dependent inhibitor since the NMDA receptor must be activated prior to the neurosteroid can bind on it. The degree of inhibition of responses of phasically activated synaptic NMDA receptors is lower than the inhibition of tonically activated recombinant NMDA receptors after a long glutamate application. This conclusion is of a particular physiological relevance because under pathological conditions extracellular levels of glutamate are likely to be tonically elevated. Prolonged activation of extrasynaptic NMDA receptors can lead to the specific cell death referred to as excitotoxicity. The use-

intensities. The average value of 10-90% rise times was 8 ± 2 ms (n = 10). The time-course of deactivation was best fit by a double exponential function with τ_{fast} = 94 ± 31 ms (60 ± 13%) and τ_{slow} = 339 ± 72 ms (n = 10). The amplitude of NMDAR EPSCs was reversibly diminished to 50 ± 10% of the control response by 5 μM ifenprodil, a high-affinity antagonist of NR2B containing NMDA receptors (Williams, 1993).

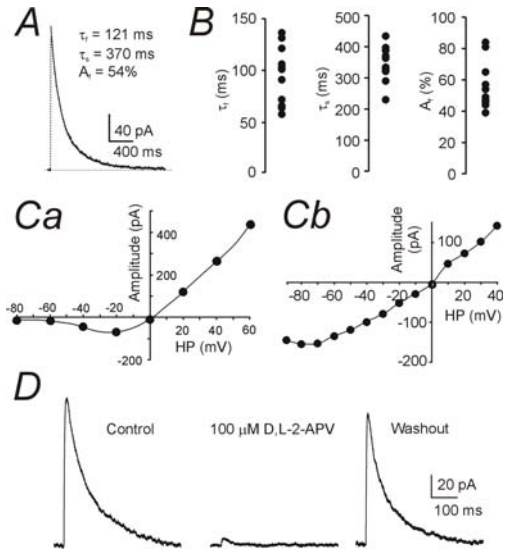

Figure 15. The excitatory synaptic transmission between primary afferent fibers and lamina I Sp5C neurons mediated by NMDA receptors. ***A,*** Average of 15 consecutive NMDAR EPSCs evoked by focal stimulation of spinal trigeminal tract (holding potential +40 mV). The deactivation of NMDA receptor-mediated EPSCs was best fit by a double exponential function with time constants and relative contribution of the fast component shown. ***B,*** Scatter plots representing the fast (τ_f) and the slow (τ_s) time constant of NMDAR EPSCs deactivation and the relative contribution of the fast component (A_f). Each point represents one neuron. ***C,*** The current-voltage relationships of NMDAR EPSCs. ***Ca,*** NMDAR EPSCs show a characteristic "J-shaped" current-voltage relationship when recorded at physiological Mg^{2+} concentration (1 mM), with the maximum amplitude of the response near -30 mV. ***Cb,*** In the presence of 1 μM Mg^{2+} the current-voltage relationship is nearly linear. HP in parts *Ca*, *Cb* means the holding potential. ***D,*** The evoked NMDAR EPSCs were highly sensitive to a competitive NMDA receptor antagonist D,L-APV (100 μM). The inhibition of responses was almost fully reversible.

When AMPA receptor-mediated EPSCs (AMPAR EPSCs) were recorded, the extracellular solution contained bicuculline methochloride (10 μM) to block $GABA_A$ receptors and strychnine (1 μM) to block glycine receptors. AMPAR mEPSCs were recorded in the presence of tetrodotoxin (TTX, 1 μM) to block voltage-dependent sodium channels, bicuculline (10 μM), and strychnine (1 μM). When NMDAR EPSCs were recorded, the extracellular solution was routinely supplemented with glycine (10 μM) to activate glycine-binding sites associated with NMDA receptors and 6-cyano-7-nitroquinoxaline-2,3-dione (CNQX; 5 μM) to block AMPA receptors. Bicuculline (10 μM) and strychnine (1 μM) were also added.

A perfusion pump, ensuring constant ECS flow rate around the slices was used. A microprocessor-controlled multibarrel fast-perfusion system, with a time constant of solution exchange around cells of ~10 ms, was used to apply test and control solutions when recording from cultured neurons (Vyklicky et al., 1990). For the purpose of studying the synaptic transmission temperature dependence, a temperature control system (Dittert *et al.* 2006) was adopted to control for the temperature (25 - 45°C) at which the EPSCs were recorded from the slice.

Experiments were performed primarily at 23-26 ^oC or, in the case of study of NMDAR EPSCs temperature dependence, at relevant temperatures associated with the design of the experiments. All drugs, unless otherwise stated, were purchased from Sigma (St. Louis, MO, USA) or Tocris Cookson Ltd. (Avonmouth, UK).

Data analysis

The data analysis was performed using the pClamp 9.0.1.24 software (Axon Instruments, USA). The results are presented as mean ± standard deviation (S.D.) with n equal to the number of cells studied. Statistical comparison of groups was carried out using one-way ANOVA, paired/unpaired t-test or the Fisher exact test; $P<0.05$ or $P<0.001$ was used to determine the statistical significance.

Input resistance (R_{in}) was calculated from voltage responses (U) induced by hyperpolarizing current injections (I; applied at 10 pA step increments) in the linear region of the current-voltage relationship as follows:

$$R_{in} = \Delta U / \Delta I \qquad \text{(Eq. I)}$$

The membrane time constant (τ_m) was determined from exponential fits of the responses to calculate R_{in} and was used to calculate membrane capacitance (C_m) according to the following equation:

$$C_m = \tau_m / R_{in} \qquad \text{(Eq. II)}$$

We evaluated the NMDAR EPSCs temperature dependence as follows. The temperature dependence of a rate constant, k(T), can be characterized in terms of either a temperature coefficient, Q_{10}, or an activation energy, E_a. The activation energy is defined by the Arrhenius equation:

$$k(T) = A \exp(-E_a / RT) \qquad \text{(Eq. III)},$$

where A is a constant, R is the gas constant and T is absolute temperature. The value of E_a can be determined from the Arrhenius plot (ln k vs. 1/T) as follows:

$$E_a = - \text{slope} * R$$

Q_{10} was calculated with the values given by the Arrhenius plot as follows:

$$Q_{10}(T) = k(T+10) / k(T)$$

As the Q_{10} is determined by the temperature, we calculated its value for 35°C.

4. Results

Temperature affects the amplitude and deactivation kinetics of NMDAR EPSCs

One of the aims of the present study was to investigate the influence of extracellular temperature on the NMDAR EPSCs. We studied the temperature dependence of evoked and miniature NMDAR EPSCs. The results of our experiments show that the amplitude and deactivation kinetics of the NMDAR EPSCs in layer II/III pyramidal neurons of the rat neocortex are temperature dependent.

Postsynaptic currents were evoked in neurons voltage-clamped at +40 mV by focal electrical stimulation of the adjacent tissue. After an initial period in which control

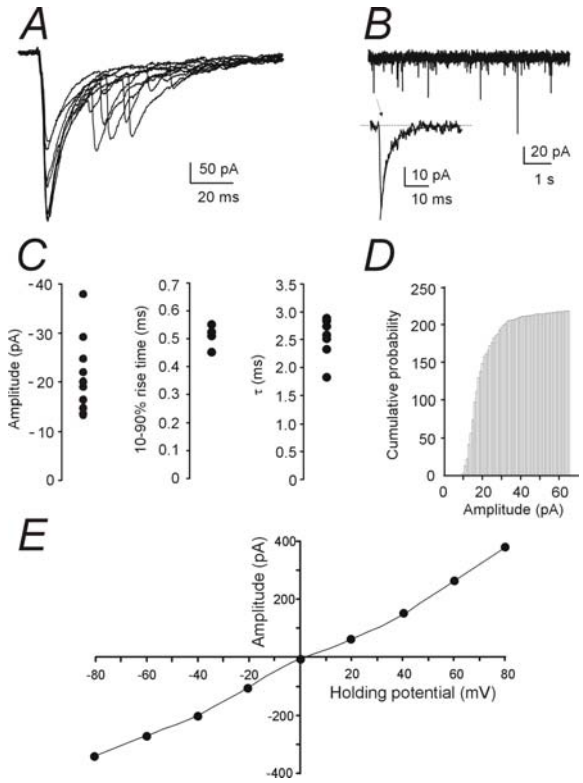

Figure 14. The excitatory synaptic transmission between primary afferent fibers and Sp5C lamina I neurons mediated by AMPA receptors. ***A,*** Eight consecutive AMPAR EPSCs evoked by focal electrical stimulation of spinal trigeminal tract are shown superimposed. An apparently monosynaptic component of AMPAR EPSCs is followed by a polysynaptic component exhibiting variable latency. ***B,*** Spontaneously occurring miniature AMPAR EPSCs recorded at -70 mV in the presence of 1 μM tetrodotoxin and inhibitory synaptic transmission blockers (see Methods for details). One selected miniature AMPAR EPSC is shown on an expanded time scale. The mean 10-90% rise time measured from 45 miniature AMPAR EPSCs in this cell was 0.50 ms and the deactivation fit by a single exponential function with the time constant τ = 2.5 ms. ***C,*** Scatter plots representing average amplitude, 10-90% rise times and deactivation time course of miniature AMPAR EPSCs (each point in graphs represents detected miniature EPSC events recorded from one neuron. ***D,*** Cumulative distribution histogram of amplitudes of miniature AMPAR EPSC with mean amplitude of –23 ± 8 pA. ***E,*** The current-voltage relationship of evoked AMPAR EPSCs was linear with the reversal potential close to 0 mV.

Evoked and pharmacologically isolated NMDAR EPSCs (see Methods for details) were recorded at a positive holding potential +40 mV (Fig. 15). Only the monosynaptic component of NMDAR EPSCs was observed at a wide-range of stimulus

extent, a part of the dendritic arborization was destroyed during the slicing process. An axon-like process could not be seen in any pyramidal neuron.

Multipolar neurons (8 of 25 analyzed cells; Fig. 13D) showed an oval or circular soma. The somata were the smallest of all groups, with a length of 10 ± 2 μm and a width of 10 ± 2 μm. Four to eight primary dendrites mostly oriented to deeper laminae of Sp5C, and there was considerably high density branching of dendrites. In one multipolar neuron, an axon-like process could be seen emerging from the soma and followed into the lamina I for a substantial distance (see the asterisk in Fig. 13D).

Our next experiments aimed at providing the basic characterization of the synaptic input to Sp5C lamina I neurons. Focal electrical stimulation (see Methods) of the spinal trigeminal tract was used to elicit EPSCs in lamina I neurons. AMPAR EPSCs were recorded at a holding membrane potential of -70 mV in the presence of bicuculine, strychnine and physiological concentration of Mg^{2+} (1 mM). The amplitude of an apparently monosynaptic component was analyzed in 15 neurons and ranged from 60 to 800 pA. This component appeared with a short latency after the stimulus and showed <0.5 ms intertrial variation. Increasing the stimulus intensity usually led only to a subtle increase in the amplitude of the first, monosynaptic component but regularly increased both the amplitude and duration of the late, apparently polysynaptic component, which made the analysis of AMPAR EPSCs kinetic properties difficult (Fig. 14A). Kinetic analysis was therefore performed on spontaneously occurring miniature AMPAR EPSCs recorded in the presence of 1 μM tetrodotoxin (see Methods for details) (Fig. 14C). The 10-90% rise time of miniature AMPAR EPSCs was 0.50 ± 0.06 ms, the decay time constant was best fit by a single exponential function with a deactivation time constant τ of 2.5 ± 0.5 ms (n = 7). The decay time was not correlated with the 10-90% rise time (r = 0.30, Spearman's rank correlation; n = 7). This indicates that the deactivation time course of miniature AMPAR EPSCs is not altered by dendritic cable properties. Analysis of the amplitude of miniature AMPAR EPSCs showed that the distribution of amplitudes varied from -10 to -118 pA, with a median of -18 pA (Fig. 14D). The mean miniature AMPAR EPSC amplitude was -23 ± 8 pA (ranging from 13 to 38 pA; n = 7).

NMDAR EPSCs were recorded at 35°C, the temperature of the perfusion solution was changed to 25, 30 or 40°C. Figure 1A shows a typical example of the NMDAR EPSCs recorded from the same neuron at different temperatures. The mean amplitude of the postsynaptic currents recorded at 25, 30 and 40°C was 65, 86, and 112% of that recorded at 35°C (see Fig. 1B filled columns).

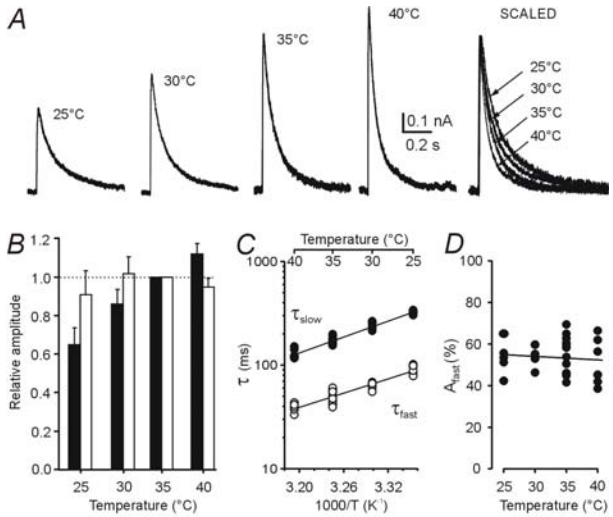

Figure 1. The effect of temperature on the amplitude and time course of evoked NMDAR EPSCs. ***A,*** Evoked NMDAR EPSCs recorded from a pyramidal layer II/III neocortical neuron voltage clamped at a holding potential of +40 mV. Warming of the perfusing ECS lead to NMDAR EPSCs amplitude increase and shortening of their deactivation kinetics. All traces (5 consecutive responses at each temperature were averaged) are superimposed and normalized in the right to show the deactivation kinetics of the postsynaptic currents with temperature changes from 25 to 40°C. All traces are from the same neuron. ***B,*** Summary of the effect of temperature on the amplitude of evoked NMDAR EPSCs. Filled bars indicate mean relative amplitude (±SD) of responses normalized with respect to the response at 35°C, and open bars represent these responses further normalized with respect to the amplitude of the single-channel currents calculated from the Arrhenius plot for the given temperature. The mean relative changes of the NMDAR EPSCs amplitude and those normalized to the single channel conductance were not significantly different (ANOVA). Error bars represent mean ±SD; the numbers of cells were 18, 12, 23 and 7 for 25, 30, 35 and 40°C, respectively. ***C,*** Arrhenius plot shows the temperature dependence of the fast and slow time constant of the NMDAR EPSCs deactivation. The line is the best fit of the data to Equation III (see Methods) and gives an E_a of 44 ± 3 kJ/mol (Q_{10} = 1.7) for the fast component of deactivation and E_a of 49 ± 2 kJ/mol (Q_{10} = 1.8) for the slow component of deactivation. ***D,*** Relative amplitude of the fast component (A_{fast}) was only weakly temperature sensitive.

Since the amplitude of NMDAR EPSCs is controlled by presynaptic and postsynaptic mechanisms, we performed next experiments to exclude the possibility that

the temperature dependence of the amplitude of the NMDAR EPSCs is influenced only by the single-channel conductance and not by other mechanisms (e.g. probability of transmitter release and channel kinetics) that counteract one another. To eliminate the presynaptic mechanism, the effect of temperature on the amplitude of miniature NMDAR EPSCs was determined (Fig. 2). Figure 2B shows a cumulative probability histogram of the amplitude of miniature NMDAR EPSCs recorded at 25, 35 and 40°C. The amplitude of miniature NMDAR EPSCs increased with temperature; however, when normalized to the single-channel conductance, no significant differences in the relative amplitude were observed (Fig. 2C, open bars).

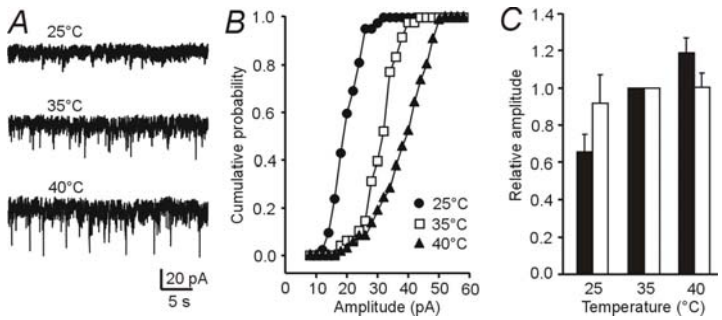

Figure 2. Effects of temperature on miniature NMDAR EPSCs. ***A,*** The miniature NMDAR EPSCs were recorded from neocortical layer II/III pyramidal neurons voltage-clamped at -75 mV in Mg^{2+}-free extracellular solution at indicated temperatures. ***B,*** Plot of cumulative probability of miniature NMDAR EPSCs amplitudes recorded at 25, 35 and 40°C. ***C,*** Summary of the effect of temperature on the miniature NMDAR EPSCs amplitude. The amplitude at 25 and 40°C was normalized to that at 35°C (filled columns) and with respect to the amplitude of the single-channel currents calculated from the Arrhenius plot at a given temperature (open columns). Error bars represent mean ±SD; the numbers of cells were 10, 13 and 7 for 25, 35 and 40°C, respectively.

The deactivation time course is essential in determining the duration of NMDAR EPSCs. We performed experiments to estimate the temperature dependence of the deactivation kinetics of NMDAR EPSCs. We demonstrate that the decay of NMDAR EPSCs recorded at 25°C was best fit by a double exponential function, which is in agreement with most papers studying the NMDAR EPSCs deactivation time course in brain slices so far. The mean time constants of NMDAR EPSCs decay recorded at 25°C

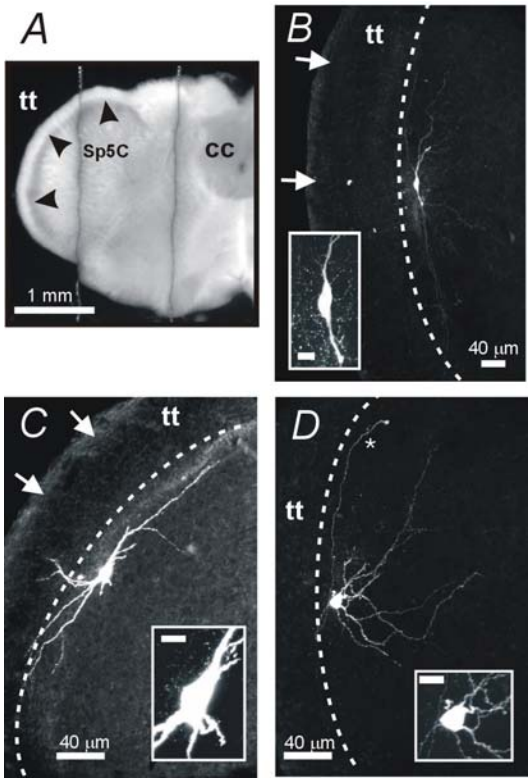

Figure 13. The brainstem transverse slice and morphology of biocytin- and Streptavidin-Alexa 488-labeled neurons. ***A,*** Slices were prepared from the medulla oblongata region, caudal to obex. The caudal part of the trigeminal nucleus (Sp5C) is located in the dorso-lateral segment. Lamina I (indicated by black arrowheads) is located at the border of the nucleus and the spinal trigeminal tract (tt); CC = central canal. Lamina I of the Sp5C comprises three distinct morphological neuronal types: fusiform ***(B),*** pyramidal ***(C)***, and multipolar ***(D)***. A three-dimensional reconstruction viewed in the coronal section plane is shown. Insets illustrate enlarged areas of neuronal somata and proximal dendrites. Scale bars of the insets represent 10 μm. The borders between lamina I and spinal trigeminal tract (tt) are marked with a dotted line. The outer boundary of the slice is indicated by white arrows. Asterisk in *D* indicates the axon. Electrophysiological recordings from cells in B, C, and D are shown in Figs. 9, 10, and 11, respectively.

Pyramidal neurons (5 of 25 analyzed cells; Fig. 13C), with a typical pyramidal cell soma 20 ± 2 μm in length and 15 ± 3 μm in width, were the largest of all morphological groups. Three primary dendrites, heading mainly towards lamina I or adjacent spinal trigeminal tract, emerged from the triangular soma. Dendritic branching was scarcer than in fusiform or multipolar neurons. It is likely that because of their large

Neurons characterized electrophysiologically in Sp5C lamina I in medulla oblongata slices (Fig. 13A) were subsequently morphologically analyzed. Cells were subdivided into three distinct morphological types: fusiform, pyramidal, and multipolar.

Fusiform neurons (12 of 25 analyzed cells; Fig. 13B) were recognized by an elongated cell soma with a length of 15 ± 3 µm and a width of 8 ± 2 µm. Two primary dendritic trunks emerged from the soma and displayed relatively sparse branching proximal to the soma. The dendritic branches were oriented along the lamina I and spinal trigeminal tract boundary. The site of the first primary dendrite bifurcation could be recognized in some fusiform neurons. The distance between the soma and the bifurcation varied among individual cells. An axon-like process, heading towards the deeper laminae of Sp5C, could be seen emerging from the primary dendrite in 2 of 12 neurons.

were τ_{fast} = 92 ± 9 ms (A_{fast} = 54 ± 9%) and τ_{slow} = 321 ± 12 ms (*n* = 7). The decay was accelerated after the temperature increase (see overlaid responses in Fig. 1A, quite in the right). An Arrhenius plot of the time constants of the deactivation indicates that both components were only weakly temperature sensitive (τ_{fast}: E_a = 44 ± 3 (Q_{10} = 1.7); τ_{slow}: E_a = 49 ± 2 (Q_{10} = 1.8)) and that their relative amplitude was virtually temperature insensitive (Figs. 1C, 1D).

It has been shown previously that the time-course of NMDAR deactivation is controlled by the receptor subunit composition (Monyer et al., 1994; Flint et al., 1997). We performed next experiments to estimate the temperature dependence of the deactivation kinetics of synaptic receptors containing NR2B subunit. It has been previously shown that EPSCs in layer II/III pyramidal neurons are mediated by NMDARs composed of NR2A and NR2B subunits, with the relative density changing as a function of postnatal age (Flint et al., 1997). This fits well with the results of our experiments, which show that NMDAR EPSCs in layer II/III pyramidal neurons at postnatal day 14 rats (PD 14) were inhibited in the presence of ifenprodil (10 µM; selective inhibitor of NR2B containing NMDA receptors; (Williams, 1993)) by 47 ± 4% (*n* = 4) and 65 ± 11% (*n* = 7) at 25 and 35°C, respectively (Fig 3A). In contrast to the amplitude, the decay time constants of NMDAR EPSCs were not significantly affected by ifenprodil at either temperature (Fig. 3B).

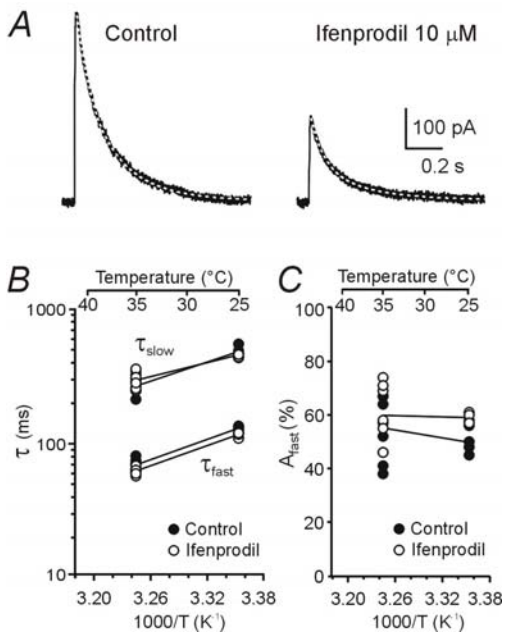

Figure 3. Effects of ifenprodil (10 μM) on NMDAR EPSCs. ***A,*** Example of NMDAR EPSC evoked at 35°C in a cortical layer II/III pyramidal neuron before (Control) and 18-20 min after the start of 10 μM ifenprodil application. The deactivation time-course was fit by a double exponential function (indicated by a dashed line); control: τ_{fast} = 68 ms (A_{fast} = 41%) and τ_{slow} = 227 ms; ifenprodil: τ_{fast} = 58 ms (A_{fast} = 46%) and τ_{slow} = 201 ms. ***B,*** Arrhenius plots of the temperature dependence of the fast (τ_{fast}) and slow (τ_{slow}) time constants of NMDAR EPSCs recorded in the presence of control ECS and ifenprodil. The time constants decreased with increasing temperature (control: τ_{fast} E_a = 44 ± 4 (Q_{10} = 1.7); τ_{slow}: E_a = 43 ± 6 (Q_{10} = 1.7); ifenprodil: τ_{fast} E_a = 41 ± 1 kJ/mol (Q_{10} = 1.6); τ_{slow}: E_a = 33 ± 5 kJ/mol (Q_{10} = 1.5)). ***C***, Relative amplitude of both components was only weakly temperature sensitive. Ifenprodil had no significant effect on either τ_{fast} or τ_{slow} recorded at 25°C (n = 4) and at 35°C (n = 7). The relative contribution of A_{fast} was significantly higher in ifenprodil, both at 25°C and 35°C.

The effects of neurosteroid 20-oxo-5β-pregnan-3α-yl sulfate (3α5βS) on NMDA receptor-mediated excitatory synaptic transmission

It has been shown previously, that chemical compounds of neurosteroidal nature occuring endogenously, such as 3α5βS or pregnenolon sulfate (PS), modulate the activity of native and recombinant NMDA receptors (Wu et al., 1991; Park-Chung et al., 1997; Horak et al., 2004). Another of the aims of our study was to investigate the effects of these compounds on the excitatory synaptic transmission mediated by NMDA receptors.

potential compared with the other groups. ***C,*** Shows instantaneous firing frequency as a function of time. ***D,*** The increasing intensity of stimulation induced a higher number of spikes with the initial delay maintained. At higher depolarization levels, one spike could occur at the beginning of the pulse. However, this spike was followed by a delay before the train of regular firing started (panel *A*, top trace). ***E,*** Time from the beginning of the depolarizing pulse to the first action potential. Delayed onset neurons (•) were characterized by a significant time span between the start of the pulse and the first action potential (at rheobase) compared with tonic (o) as well as phasic and single spike neurons.

Single spike neurons (4 of 25 analyzed neurons) fired only a few action potentials at intermediate and high stimulus intensities (Fig. 12A). Even at very high stimulus intensities (~300 pA), these neurons fired only a few action potentials (1-5) generated during the first half of the stimulus-induced depolarization (Fig. 12C).

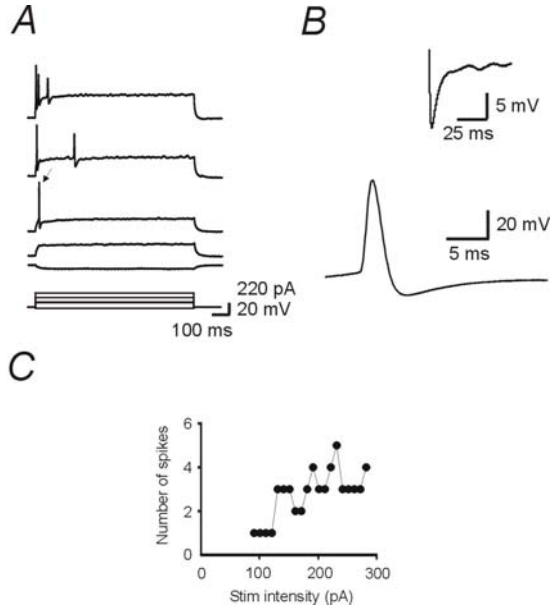

Figure 12. Intrinsic membrane properties of a neuron with a "single" spike pattern of firing. ***A,*** 900 ms hyperpolarizing and depolarizing current pulses (-20, +80, +90, +170, +250 pA) from resting membrane potential (-60 mV). ***B,*** The action potential shown in *A* on an expanded time and voltage scale. The afterhyperpolarization was monophasic in single spiking neurons. ***C,*** The total number of spikes elicited by depolarization (even at levels as high as 300 pA) was always lower than or equal to five.

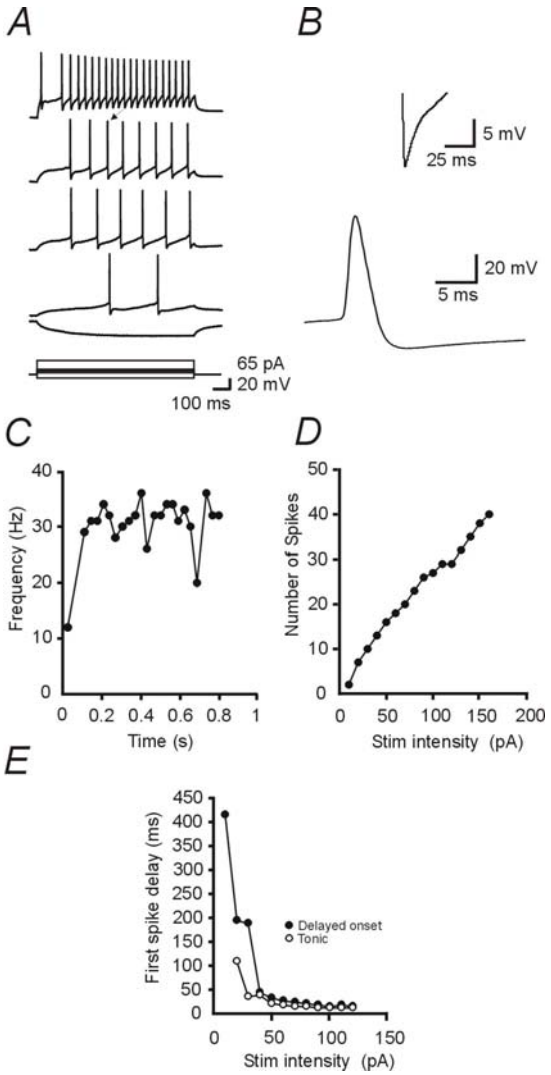

Figure 11. Intrinsic membrane properties of a neuron with a delayed onset of spiking. *A,* 900 ms steps of current injections (-20, +10, +20, +30, +120 pA) from resting membrane potential (-77 mV). Depolarizing current injections evoked a series of action potentials, beginning with a delay of several hundred milliseconds at low and intermediate stimulus intensities. ***B,*** One selected action potential is shown (designated by an arrow in *A*) on an expanded scale. In the inset the shape of afterhyperpolarization is shown. Note larger half width of the action

In our experiments we characterized the effects of 3α5βS on the amplitude and deactivation kinetics of NMDAR EPSCs in layer II/III pyramidal neurons of the rat cortex. After an initial period, in which control NMDAR EPSCs were recorded, the perfusion solution was exchanged for extracellular solution containing 3α5βS for a period sufficient to produce a steady state effect on the amplitude of the EPSCs (usually 15-25 min). Figure 4A shows a typical example of the effect of 100 μM 3α5βS on the amplitude and time-course of NMDAR EPSCs. In the presence of 3α5βS, the amplitude of NMDAR EPSCs slowly decreased and reached ~50% of the amplitude before the neurosteroid application. The effect was slowly reversible, presumably attributable to a slow diffusion of the neurosteroid from the slice (Fig. 4B). Taking into account the profound inhibitory effect of 3α5βS on NMDA- and glutamate-induced whole-cell responses recorded from both neurons and HEK293 cells (Petrovic et al., 2005), it was surprising that the inhibitory effect of 3α5βS on the amplitude of NMDAR EPSCs was significantly smaller at all neurosteroid concentrations tested (30-300 μM) (Fig.4C). The difference in the relative degree of 3α5βS-induced inhibition of steady-state agonist-evoked responses and NMDAR EPSCs was more pronounced at low neurosteroid concentrations.

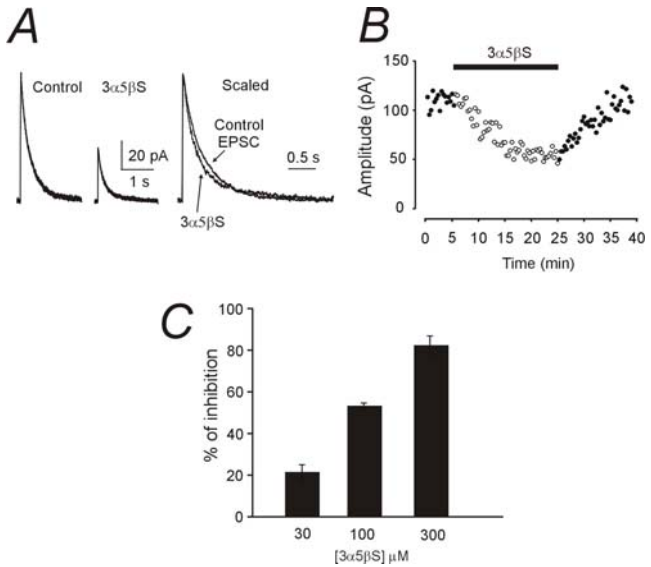

Figure 4. The effect of 3α5βS on NMDAR EPSCs. *A*, Example of NMDAR EPSC (4 consecutive responses were averaged) evoked in a cortical lamina II/III pyramidal neuron voltage clamped at +40 mV before (Control) and 23-25 min after the start of 100 μM 3α5βS application. In the right, both responses are displayed normalized to the peak amplitude of the control response and overlaid, to show the difference in the deactivation time-course. ***B*,** Plot of the amplitude of NMDAR EPSCs as a function of time of recording. Filled bar indicates duration of 100 μM 3α5βS application (same neuron as in *A*). ***C*,** Summary of the effect of 3α5βS (30 - 300 μM) on the amplitude of NMDAR EPSCs (n = 5 for each concentration). Error bars represent mean ± SD.

The decay of NMDAR EPSCs recorded in the control extracellular solution was best fit by a double exponential function with mean time constants τ_{fast} = 108 ± 36 ms (A_{fast} = 46 ± 7%) and τ_{slow} = 369 ± 21 ms (*n* = 9). In the presence of 3α5βS (100 or 300 μM), the deactivation of NMDAR EPSCs had complex kinetics characterized by an accelerated initial and decelerated late component (see overlaid responses in Fig. 4*A*). Similar effect of the neurosteroid on the deactivation time-course of NMDA receptor-mediated EPSCs was observed in all 10 neurons analyzed.

The effects of neurosteroid pregnenolon sulfate (PS) on NMDA receptor-mediated excitatory synaptic transmission and on native NMDA receptors

It has been shown previously, that PS acts as a positive modulator of native and recombinant NMDA receptors (Wu et al., 1991; Horak et al., 2004). We studied the

Figure 10. Intrinsic membrane properties of a neuron with phasic pattern of spiking. *A*, Responses were induced by current injections (-20, +10, +20 and +60 pA) from the resting membrane potential (-67 mV). Depolarization induced a train of action potentials starting at the beginning of the pulse and ceasing before the end of the pulse. ***B*,** An enlarged view of action potential (designated by an arrow in *A*). Phasically firing neurons showed a monophasic shape of afterhyperpolarization. ***C*,** Graph of the instantaneous spike frequency as a function of duration of the depolarization induced by 130 pA current injection. ***D*,** Scatter plot of the total number of spikes fired during a 900 ms depolarizing pulse as a function of stimulus intensity. ***E*,** Time from the last action potential to the end of the depolarizing pulse as a function of stimulus intensity. Phasic neurons (●) fired an initial burst of action potentials in the first half of the pulse. By contrast, tonic neurons (o) fired action potentials regularly during the entire pulse.

Neurons with delayed onset of action potentials (5 of 25 analyzed neurons) fired repetitive action potentials with a delay of several hundred milliseconds after the onset of depolarization induced by a low to intermediate stimulus intensity (Fig. 11A,E). The number of action potentials increased with increasing stimulus intensities; however, the delay was always clearly distinguishable (Fig. 11A). At higher stimulus intensities, a single action potential occurred occasionally at the very beginning of the pulse and, after a delay, was followed by a burst of action potentials. In contrast to the exponential decrease in the instantaneous firing frequency of action potentials observed in tonic and phasic neurons, delayed onset neurons showed an initial increase followed by a steady state or a slight decrease (Fig. 11C).

of action potentials throughout the depolarizing pulse increased. There was a tendency toward saturation of the spike frequency at very high stimulus intensities. Similar to what was found with tonic neurons, the instantaneous firing frequency of action potentials in phasic neurons decreased exponentially with increasing stimulus intensities (Fig. 10C).

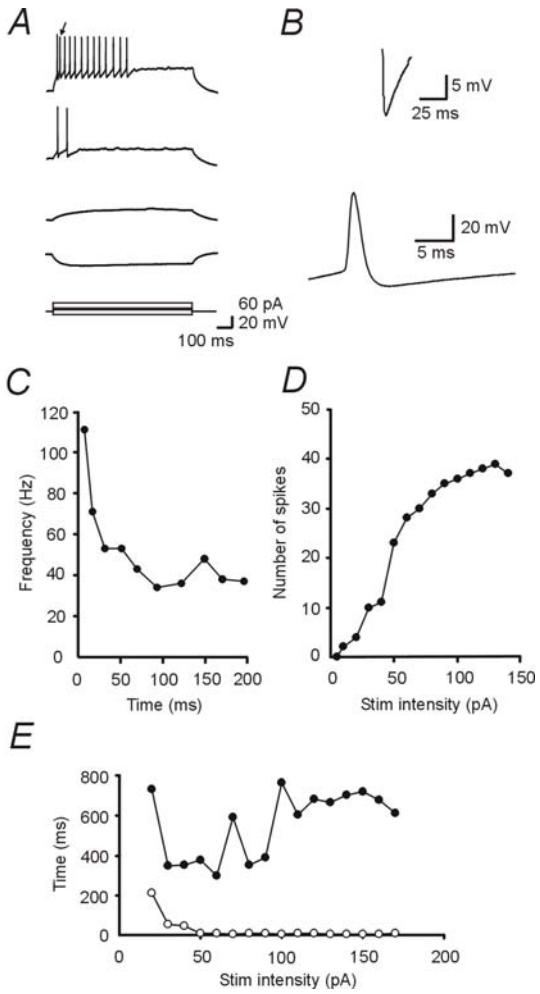

effect of PS on NMDAR EPSCs amplitude and deactivation time course in layer II/III pyramidal neurons of the rat neocortex and lamina I neurons of the Sp5C.

Figure 5 shows a typical example of the effect of 100 μM PS on the NMDAR EPSCs. Surprisingly, neither in the neocortex, nor in the Sp5C was the amplitude of EPSCs significantly increased. The average relative amplitudes of evoked EPSCs compared to control ones were 103 ± 9% (n = 10; paired t-test) in the neocortex, and 100 ± 3% (n = 4; paired t-test) in the Sp5C lamina I neurons.

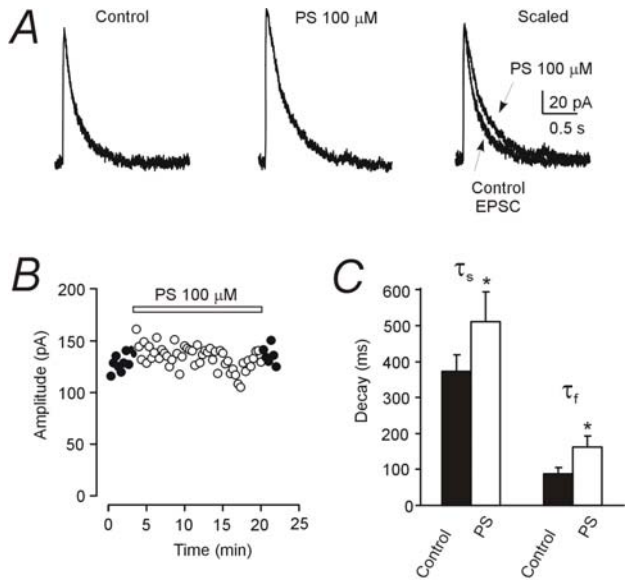

Figure 5. The effect of PS on the evoked NMDAR EPSCs in layer II/III pyramidal neurons in the neocortex. ***A,*** An example of evoked NMDAR EPSCs (5 consecutive responses were averaged) voltage clamped at +40 mV before (Control) and after 100 μM PS application. In the right, both responses are displayed normalized to the peak control response amplitude and superimposed, to show the difference in the deactivation time-course. The deactivation time course of the EPSCs could be best described by a double exponential function (control responses: τ_{fast} = 92 ms, τ_{slow} = 319 ms, A_{fast} = 56%; PS: τ_{fast} = 193 ms, τ_{slow} = 555 ms, A_{fast} = 75%). We demonstrated that PS significantly prolongs both, the fast and the slow deactivation time constants of evoked NMDAR EPSCs. ***B,*** Scatter plot of the amplitude of NMDAR EPSCs as a function of time of recording. Open bar indicates duration of 100 μM PS application, every single circle represents individual EPSC (same neuron as in *A*). ***C,*** Summary bar graph showing the effect of 100 μM PS (open bars) on the fast (τ_f) and the slow (τ_s) deactivation time constants of NMDAR EPSCs. Both, τ_f and τ_s were significantly prolonged after PS application (paired t-test, n = 5). Error bars represent mean ± SD.

In addition to the amplitude we investigated the effect of PS on the deactivation time course of the NMDAR EPSCs as well. The results of our experiments have shown that the NMDAR EPSCs decay in the neocortex and the Sp5C are best fit by a double exponential function both, for the control responses and PS affected responses. The application of 100 μM PS significantly prolongs the fastand slow component of the deactivation of NMDAR EPSCs (Fig. 5C).

It has been shown previously that PS potentiates NMDA responses in cultured hippocampal neurons. Therefore, the next experiments were performed to investigate if PS modulates synaptic NMDA receptors in cultured hippocampal neurons. We evoked NMDAR EPSCs by stimulation of a presynaptic neuron in paired recordings from neurons in hippocampal culture. The results of these experiments showed that the amplitude of pharmacologically isolated NMDA component of the excitatory postsynaptic currents was increased only slightly (5 ± 11%, $n = 4$, paired t-test) after 100 μM PS application (see Fig. 6).

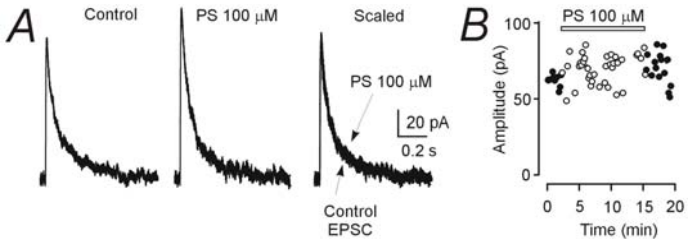

Figure 6. The effect of 100 μM PS on NMDAR EPSCs recorded from pairs of cultured hippocampal neurons. ***A,*** An example of the EPSC from a pair of neurons with the postsynaptic cell voltage-clamped at +40mV before (Control) and after 10-12 minutes of PS application. In the right, both EPSCs are shown normalized to the control response and superimposed. ***B,*** Scatter plot of the amplitude of NMDAR EPSC as a function of time of recording. Open bar indicates duration of 100 μM PS application, every single circle represents individual EPSC (same pair of neurons as in *A*).

Based on the results described above and on the results published previously (Bowlby, 1993; Horak et al., 2004), it is likely that synaptic and non-synaptic NMDA receptors could be affected by PS differently. Therefore we performed next experiments, in which we tried to change the degree of PS potentiation of NMDA induced responses

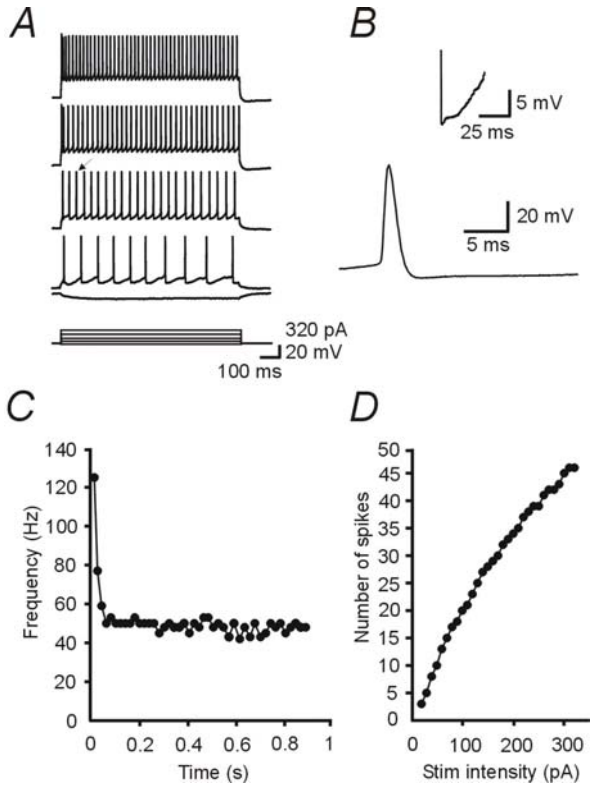

Figure 9. Intrinsic membrane properties of a neuron with tonic pattern of spiking. ***A,*** A series of hyperpolarizing and depolarizing current pulses (-20, +50, +120, +220 and + 320 pA) from resting membrane potential (-59 mV). Current injections induced a train of action potentials throughout the depolarizing pulses. ***B,*** One selected action potential (designated by an arrow in *A*) is shown on an expanded time and voltage scale. These neurons showed a biphasic shape of afterhyperpolarization. ***C,*** The instantaneous firing frequency is shown as a function of the duration of the depolarization induced by 300 pA current injection. ***D,*** Graph of the total number of spikes fired during a 900 ms depolarization step is plotted as a function of the stimulation intensity.

Neurons with phasic spiking (4 of 25 analyzed neurons) fired action potentials at low stimulation intensities; however, unlike the tonic neurons, they exhibited only one or two action potentials at the onset of the stimulus. At intermediate stimulus intensities (≤120 pA), phasic neurons fired a burst of action potentials which terminated before the end of the stimulus (Fig. 10A,E). At higher stimulus intensities (>120 pA), the number

the whole-cell configuration. For the morphological analysis we labeled each neuron with a fluorescent biocytin-Streptavidin-Alexa 488 complex.

Electrophysiological examination of Sp5C lamina I neurons indicated that this cell population is physiologically heterogeneous, differing in both passive and active membrane properties. The most distinguishable difference was the pattern of action potentials firing in response to somatic current injections. Four groups of neurons - tonic, phasic, delayed onset, and single spike - were identified on the basis of this characteristic (see Figs. 9-12).

Neurons with tonic spiking (12 of 25 analyzed neurons) were easily excited and fired action potentials regularly throughout the depolarizing current pulse (900 ms) (Fig. 9A). They fired tonically at very low depolarization levels and, as the stimulation intensity increased, the number of action potentials increased linearly (Fig. 9D). Some tonic neurons (n = 9; 69%) reached saturation in the spike frequency at stimulus intensities >250 pA, while others (n = 4; 31%) did not reach saturation even at high stimulus intensities of 300 – 420 pA. Although the tonic cells fired throughout the depolarization, the instantaneous firing frequency of action potentials decreased exponentially with stimulus intensities (Fig. 9C).

in cultured hippocampal neurons by various treatments to attempt to reveal possible cellular mechanisms causing this discrepancy.

The control responses induced by 100 μM NMDA recorded in the presence of bicuculine, strychnine and TTX from hippocampal neurons were potentiated 2.85 ± 0.23-fold (n = 20) after 300 μM PS pre-application and subsequent co-application with NMDA. We used the protocol of PS pre-application (25 s) and subsequent co-application (Horak et al., 2004) with 100 μM NMDA routinely in these and following experiments.

NMDA receptors were shown to exist in phosphorylated or dephosphorylated states *in vivo*. Our next experiments were therefore focused at the role of NMDA receptors phosphorylation for the degree of PS potentiation of NMDA induced responses in cultured hippocampal neurons. For the purpose of these experiments, we used staurosporine, which is a nonspecific inhibitor of various protein kinases (Tamaoki et al., 1986; Ruegg and Burgess, 1989; Yanagihara et al., 1991). Staurosporine was applied in concentrations 0.25 and 0.5 μM in incubation medium to inhibit protein kinases in neurons. The total incubation time with staurosporine was 1 to 3 hours and we used the same concentration for the application solutions as well. The results of these experiments suggest that phosphorylation/dephosphorylation could represent one of the factors influencing the degree of PS induced potentiation as this was significantly decreased on average by 35% ($P<0.001$, unpaired t-test, n = 5, Fig. 7*A,B*) after staurosporine treatment. The degree of PS induced potentiation analyzed in two neurons from sister culture, which were not treated with staurosporine, showed the degree of potentiation similar to control recordings.

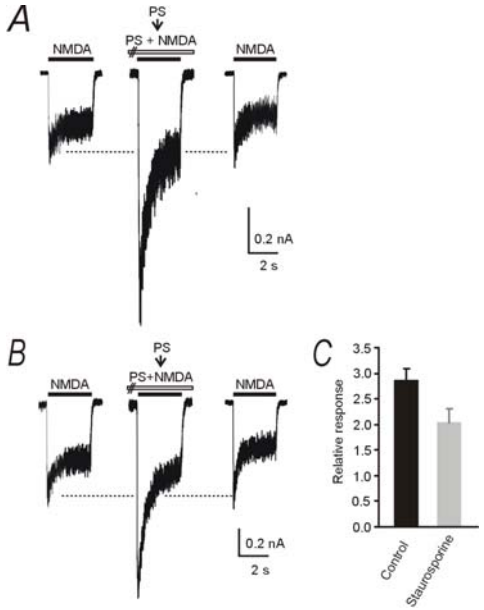

Figure 7. The incubation of cultured hippocampal neurons with staurosporine causes reduction of the degree of PS induced potentiation. ***A,*** NMDA responses of a neuron voltage-clamped at -70 mV after pre-application (25 s) and subsequent co-application of PS (300 μM) and NMDA (100 μM) obtained from a sister culture neurons without staurosporine treatment showed the same degree of potentiation as control recordings. ***B,*** NMDA responses of a neuron after pre-application and subsequent co-application of PS (300 μM) and NMDA (100 μM) obtained from a neuron treated with staurosporine (0.5 μM) for 2 hours at 37°C. Same staurosporine concentration was used in the perfusion and application solutions. ***C,*** Bar graph summarizing the relative degree of PS potentiation of NMDA responses in hippocampal neurons in culture under control conditions (black bar) and after staurosporine treatment (grey bar). There was a significant difference in the degree of PS induced potentiaton among control and staurosporine treated neurons ($P<0.001$, unpaired t-test, $n = 5$). Error bars represent mean ± SD.

As the results of our previous experiments suggest that the degree of PS potentiation may be influenced by some intracellular mechanisms, we decided to perform experiments, in which we studied the effects of PS on NMDA responses recorded from membrane patches isolated from cultured hippocampal neurons.containing several NMDA receptors. Application of 100 μM NMDA onto the membrane patches evoked responses in the order of tens of picoamperes. 300 μM PS pre-application (10 s) and subsequent co-application with 100 μM NMDA caused

potentiation of the control responses by 111 ± 11% ($n = 7$, Fig. 8A) in the case PS was applied shortly after the patch isolation (<< 1 min). After two minutes of recording, however, the degree of potentiation decreased rapidly and finally disappeared completely (Fig. 8B).

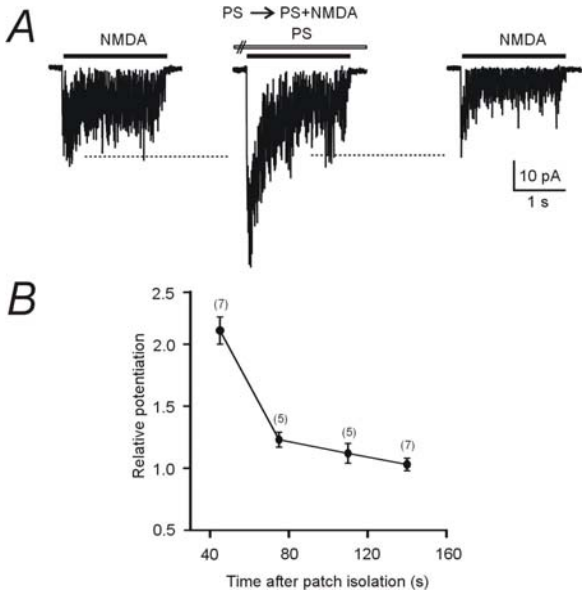

Figure 8. The effect of PS (300 μM) on the amplitude of NMDA responses recorded from isolated outside-out patches. ***A,*** Examples of NMDA responses in an outside-out patch isolated from a cultured hippocampal neuron voltage clamped at -75 mV. The pre-application of PS (300 μM) for 10 s and subsequent co-application with NMDA (100 μM) induced potentiation of NMDA responses when PS was applied in << 1 minute after the patch was isolated. ***B,*** Scatter plot showing the diminution of the degree of potentiation of NMDA responses in outside-out patches with time. When PS was applied two or more minutes after the patch isolation, the potentiation was strongly reduced or competely disappeared. The numbers in parentheses represent the numbers of patches analysed, error bars represent mean ± SD.

Electrophysiological and morphological characteristics of lamina I neurons of the caudal part of the trigeminal nucleus (Sp5C)

Cells for the following experiments were selected from Sp5C lamina I. The passive membrane properties of these neurons were recorded in current-clamp mode in